

Periodic Steady Vortices in a Stagnation Point Flow II

By **OLIVER S. KERR**

Department of Mathematics, City University†,
Northampton Square, London EC1V 0HB, UK

(Received 1997)

Steady-state perturbations to a stagnation point flow of the form $\mathbf{U} = (0, A'y, -A'z)$ are known which consist of a periodic array of counter-rotating vortices whose axes are parallel to the y -axis and which lie in the plane $z = 0$. A new understanding of how these vortices depend on the supply of incoming vorticity from afar has led to the discovery of new families of steady-state periodic vortices that can exist in a stagnation point flow. These new flows have a greater variety of structures than those previously known.

An understanding of the linkage between the vortices and the weak inflow of vorticity can have important implications for situations where such vortices are observed.

1. Introduction

A stagnation point flow of the form $\mathbf{U} = (0, A'y, -A'z)$ has been shown to be unstable to three-dimensional disturbances (Aryshev, Golovin & Ershin, 1981, Lagnado, Phan-Thien & Leal, 1984, Craik & Criminale, 1986). In Kerr & Dold (1994), hereafter referred to as KD, a family of steady-state nonlinear perturbations to this flow were found that satisfied the Navier-Stokes equation for an incompressible fluid. These consist of a periodic row of counter-rotating vortices whose cores lie on the plane $z = 0$, with axes parallel to the y -axis, and which decay as $z \rightarrow \pm\infty$. These solutions have the feature that the perturbations to the background stagnation point flow are uniform in the y -direction, and that there is no component of the perturbation velocity in this direction. In this paper we will look at some of the features of these steady solutions in more detail, and show how there is a far more extensive family of steady state perturbations to this stagnation point flow than those presented in KD. These further solutions follow from an improved understanding of the important rôle of vorticity in the formation of these vortices which was not fully appreciated at the time of writing of KD.

For a more extensive review of the relevant literature see KD.

In section 2 we will look at the way the vorticity decays as $z \rightarrow \pm\infty$, showing how there must be an algebraically decaying tail. In section 3 we will present some further families of steady vortices which will give an indication of the many further possibilities for solutions. In section 4 we will look at the relationship between the algebraically decaying tail of vorticity and the amplitude, and in section 5 we will discuss the results, including implications for growing periodic vortices in a stagnation point flow.

† Now City St George's, University of London. Contact o.s.kerr@city.ac.uk.

2. Governing equations

Any perturbation to a stagnation point flow of the form $\mathbf{U} = (0, A'y, -A'z)$ that initially has no y -dependency will always have no y -dependency. If such a perturbation initially has no velocity component in the y -direction then it will remain like this. The perturbation velocity will then be a 2-dimensional incompressible motion parallel to the x - z plane. The non-dimensional governing equations for such a perturbation to a stagnation point flow of the above form derived in KD are

$$-\frac{\partial\psi}{\partial z}\frac{\partial\omega}{\partial x} + \frac{\partial\psi}{\partial x}\frac{\partial\omega}{\partial z} - \lambda z\frac{\partial\omega}{\partial z} - \lambda\omega = \left(\frac{\partial^2}{\partial x^2} + \frac{\partial^2}{\partial z^2}\right)\omega, \quad (2.1)$$

where the stream function for the perturbation velocity is $\psi(x, z)$ such that the perturbation velocity is given by

$$\mathbf{u} = (u, 0, w) = \left(-\frac{\partial\psi}{\partial z}, 0, \frac{\partial\psi}{\partial x}\right), \quad (2.2)$$

and the vorticity, ω , is

$$\omega = -\left(\frac{\partial^2}{\partial x^2} + \frac{\partial^2}{\partial z^2}\right)\psi. \quad (2.3)$$

The above sign conventions (required by a referee of KD) result in ω being the component of vorticity in the *negative* y -direction.

The length scale used for the nondimensionalisation is k^{-1} , where the assumed periodicity of the vortices in the x -direction is $2\pi/k$. The stream function is scaled with the kinematic viscosity, ν . The nondimensional parameter

$$\lambda = \frac{A'}{\nu k^2} \quad (2.4)$$

is a measure of the strength of the converging flow compared to the rate of viscous dissipation.

We can expand the periodic solutions in terms of Fourier series in the x -component:

$$\omega(x, z) = \sum_{n=0}^{\infty} a_n(z) \cos nx + b_n(z) \sin nx, \quad (2.5a)$$

$$\psi(x, z) = \sum_{n=0}^{\infty} c_n(z) \cos nx + d_n(z) \sin nx. \quad (2.5b)$$

Unlike KD, we allow the possibility for all the functions $a_n(z)$, $b_n(z)$, $c_n(z)$ and $d_n(z)$ to be non-trivial. These Fourier series are substituted into (2.1) and (2.3), giving rise to an infinite set of ordinary differential equations

$$a_n'' + \lambda z a_n' + (\lambda - n^2)a_n = J_n(\psi, \omega), \quad (2.6a)$$

$$b_n'' + \lambda z b_n' + (\lambda - n^2)b_n = K_n(\psi, \omega), \quad (2.6b)$$

$$c_n'' - n^2 c_n = -a_n, \quad (2.6c)$$

$$d_n'' - n^2 d_n = -b_n, \quad (2.6d)$$

where $J_n(\psi, \omega)$ and $K_n(\psi, \omega)$ are the appropriate nonlinear terms. This system of equations was truncated as before, and solved using a fourth order Runge-Kutta scheme. As in KD we will require all perturbation velocities to decay to 0 as $z \rightarrow \pm\infty$. For large $|z|$ a shooting scheme was used to ensure that the functions decayed with the correct asymptotic behaviour (see the next section).

In KD it was found that satisfactory convergence could be obtained if the system of equations was truncated after $n = 12$. For some of the examples in this current work it was necessary to continue up to $n = 48$. One test of convergence was to examine the amplitudes of the vorticity at the cores and in the far field. The ratio of these would only converge once the accuracy was sufficient to resolve some of the finer scale structures in the vorticity seen in some of the large amplitude solutions discussed in section 5. This linkage between the amplitude of the vortices and the far field was not investigated in KD, hence a lower resolution was adequate there.

3. Large $|z|$ behaviour

The behaviour of the decaying vorticity as $z \rightarrow \pm\infty$ plays a crucial rôle in the form of the periodic vortices that was not appreciated in KD. The large $|z|$ behaviour of the vorticity tail for the Fourier mode proportional to $\cos nx$ (or $\sin nx$), where the nonlinear terms can be neglected, satisfies the linearised equation

$$a_n'' + \lambda z a_n' + (\lambda - n^2)a_n = 0. \quad (3.1)$$

This equation has two possible sorts of leading order behaviour in the large $|z|$ limit. As $z \rightarrow \infty$ either

$$a_n \sim Bz^{-(\lambda-n^2)/\lambda} \quad (3.2)$$

or

$$a_n \sim C \int_z^\infty e^{-\lambda z'^2/2} dz'. \quad (3.3)$$

The second of these is the behaviour found in the similarity solutions of Lin & Corcos (1984). The behaviour in (3.2) may at first seem unexpected. However, if one considers the behaviour of vorticity with this assumed periodicity in the x -direction, and no variation in the z direction then it will be found to grow exponentially in time due to vortex stretching as

$$\omega \propto \exp(\lambda - n^2)t. \quad (3.4)$$

Far from $z = 0$ the z variation of the vorticity is weak, and so a parcel of vorticity will indeed grow with approximately this growth rate. However, the parcel is also being advected towards the plane $z = 0$ with velocity $-\lambda z$, and so its distance from the plane $z = 0$ will vary with time as $\exp(-\lambda t)$. Thus the vorticity as a function of z will behave as

$$\omega \propto z^{-(\lambda-n^2)/\lambda}. \quad (3.5)$$

This is the behaviour found in (3.2). Thus the algebraic tail to the vorticity is a manifestation of the vorticity growing exponentially as it approaches $z = 0$. As the vorticity approaches the plane of symmetry the length scale in the z -direction decreases thus increasing the rate of viscous dissipation, and limiting further growth.

If we look at the equations for linear perturbations we find that non-trivial solutions can have the super-exponential decay for either positive or negative z but not both. This can be seen by integrating (3.1) between two limits, say $z = \alpha$ and $z = \beta$, to give

$$a_n'(\beta) - a_n'(\alpha) + \lambda\beta a_n(\beta) - \lambda\alpha a_n(\alpha) - n^2 \int_\alpha^\beta a_n(z) dz = 0. \quad (3.6)$$

From this equation we can deduce a series of results.

The first result is that no solutions exist with more than one zero. For example, if we assume that we have a solution which is positive between two zeros at α and β , with

$\alpha < \beta$, then the first two terms cannot be positive, and the next two terms are zero. There are no positive contributions to balance the final negative integral term. Hence we conclude it is not possible for there to be a function $a_n(z)$ which satisfies (3.1) and has two zeros.

The second result is that we cannot have a zero and superexponential decay in either direction. For example if we have a zero at $z = \alpha$ with $a_n(z) > 0$ for $z > \alpha$ and assume fast decay for large positive z , then looking at the limit as $\beta \rightarrow \infty$ in (3.6) would give the first and third terms both tending to 0 rapidly, the second term would be non-positive, and the fourth term zero. Again there is nothing to balance the negative contribution from the integral. This result can be extended to both directions, and so we conclude that if $a_n(z)$ has a zero then it must decay algebraically in both directions.

The last result is that we cannot have a one-signed function with two rapidly decaying tails. If we had a positive function which behaved in this way, and we looked at the limits as $\alpha \rightarrow -\infty$ and $\beta \rightarrow \infty$, then the first four terms of (3.6) must all tend to 0, and so the integral of $a_n(z)$ must also be zero. This is not possible for a positive function, so we conclude that we must have at least one algebraically decaying tail.

The behaviour described above is useful in understanding the possible solutions to the governing equations. We see that without a supply of vorticity being swept towards the plane $z = 0$ there would be no steady-state vortices. A similarity solution for the case with rapidly decaying vorticity in both directions was found by Lin & Corcos (1984). Their solutions were all exponentially decaying with time. We can regard the vortices observed near the plane $z = 0$ as being the result of the vorticity that is supplied at some point a long way from this plane. In KD it was assumed that the fundamental mode of the vorticity was an even function in z and the numerical solutions were found by imposing the maximum value of the stream function at the origin and allowing vorticity in the algebraic tail of the fundamental mode to decay as appropriate. This choice was made based on the original expected form of the vortices. This assumption gave rise to solutions where the vorticity tail from negative z and that from positive z were of the same magnitude and with incoming positive vorticity aligned. It would be equally possible to have the vorticity tails of opposite signs, in which case the fundamental mode would still consist of the same Fourier modes, but the fundamental modes of the vorticity and stream function would be odd functions in z . Alternatively there could be considered to be an arbitrary shift in the alignment between the incoming vorticity. These are some of the additional possibilities which will be examined in the next section.

4. Further periodic vortices

In general it is possible to specify the size of the algebraically decaying tails of each mode of vorticity that satisfies the condition $n^2 < \lambda$ arbitrarily as $z \rightarrow \pm\infty$. There is a vast potential range of such solutions. However, we will restrict ourselves to situations where only the fundamental modes $\cos x$ and $\sin x$ have non-zero tails coming in from infinity. It is these modes which have the greatest amplification of the vorticity as it is swept towards $z = 0$ and so would be expected to dominate. We can write the leading order behaviours of the two tails as

$$\omega \sim -A_+ z^{-(\lambda-1)/\lambda} \cos(x - \phi_+) \quad \text{as} \quad z \rightarrow +\infty, \quad (4.1a)$$

$$\omega \sim -A_- |z|^{-(\lambda-1)/\lambda} \cos(x - \phi_-) \quad \text{as} \quad z \rightarrow -\infty. \quad (4.1b)$$

We will refer to the coefficients A_+ and A_- as the amplitudes of the respective algebraic tails, and $\Phi = (\phi_+ - \phi_-)$ as the phase difference between the tails. There is no requirement

here that the amplitudes are both positive. This means that these quantities are not uniquely defined, but the convenience of this extra degree of freedom will be apparent in the subsequent subsections.

In the following subsections we will look at three of these families of solutions. In each case we will restrict ourselves to the case of $\lambda = 6$. This is the same choice used in KD to look at the variation of amplitudes of the vortices presented there.

In the first section we will look at solutions where the incoming vorticity is aligned and of equal magnitude, but of opposite sign. In the next we will still keep the incoming vorticity aligned but vary the relative strengths of the incoming vorticity. Lastly we will keep the amplitudes of the incoming vorticity the same from both directions, but allow an arbitrary phase shift between the incoming streams.

4.1. Vorticity tails aligned with opposite magnitudes

The flows found here have perturbation stream functions and vorticity that can be described in terms of the same Fourier modes as in KD:

$$\omega(x, z) = \sum_{n=1}^{\infty} a_n(z) \cos(2n-1)x + b_n(z) \sin 2nx, \quad (4.2a)$$

$$\psi(x, z) = \sum_{n=1}^{\infty} c_n(z) \cos(2n-1)x + d_n(z) \sin 2nx. \quad (4.2b)$$

With only the $\cos x$ mode decaying algebraically as $z \rightarrow \pm\infty$ all the Fourier modes omitted from the general expansion (2.5a–2.5b) are identically zero (see KD). This time the functions $a_n(z)$ and $c_n(z)$ are odd while the functions $b_n(z)$ and $d_n(z)$ are even. We will have equal tail amplitudes ($A_+ = A_-$), and a phase difference $\Phi = \pi$ (or alternatively $A_+ = -A_-$ and $\Phi = 0$). As in KD we will define the amplitude of the solutions as the maximum value of the stream function $\psi(x, z)$. This maximum may no longer be situated at the origin. A typical sequence of flows is shown in figure 1. These are calculated for $\lambda = 6$. Initially the perturbation vorticity is not sufficiently strong to induce a swirling motion in the total flow. As the amplitude increases, pairs of vortices appear. These move further away from the plane $z = 0$ as the swirling motion becomes stronger.

As the amplitude of the odd solutions increases the vortices appear to pair up and then move away from the plane of symmetry. The mechanism behind this behaviour is outlined in figure 2. The influence of each vortex's mirror image in the plane $z = 0$ is to induce a horizontal displacement in the vortices which alternates in direction between adjacent vertical pairs (figure 2(a)). The vortices in line above the z -axis are now no longer evenly spaced, and each vortex is more strongly influenced by its nearest lateral neighbour, and experiences a net tendency to move into the incoming flow (figure 2(b)). This tendency to move away from the plane of symmetry is limited by the stronger inflow as $|z|$ increases (figure 2(c)).

The linear analysis for the structure of the vortices in KD in the large λ limit is readily adapted to these solutions, and also to those of the next two sections. The analysis is not repeated here.

4.2. Vorticity tails aligned with arbitrary magnitudes

If we fix the phase difference between the tails to be zero, i.e. $\Phi = 0$, but allow the amplitude of the tails to take arbitrary values we are able to incorporate both the solutions of KD and those of the previous section. The same Fourier modes as before will be non-zero, but now there is no restriction of the symmetry of the functions $a_n(z)$, $b_n(z)$, $c_n(z)$ and $d_n(z)$. A sequence of such flows is shown in figure 3. These flows all have the amplitude

of the tails from large positive z fixed at $A_+ = 10$, but with the opposing tails having amplitudes ranging from $A_- = -10$ to $A_- = 10$. Initially two pairs of vortices are visible such as those seen in the previous section. As the magnitude of the lower vorticity tail decreases, the lower pair rapidly cease to exist, although the associated local maxima and minima of vorticity continue to exist for some time. As A_- increases the remaining pair of vortices grow until they eventually recover the form of the vortices investigated in KD.

A feature that is clear in the sequence in figure 3 is the great disparity between the strength of the vortices when the tails have the same signs and when they have opposite signs. When the tails have opposite signs there is a region of enhanced viscous dissipation near $z = 0$ where the regions of opposite vorticity are being swept together. This region is not present when the tails are of the same sign.

The double vortices of the previous subsection are quickly swamped as the amplitude of the lower tail increases, although the vorticity only becomes single-signed in each half-period when $A_- = 0$. For the majority of possible values of the lower tail the vortices closely resemble those associated with tails of the same magnitude and sign. The most noticeable difference is a slight shifting of the vortex cores above the plane $z = 0$. This displacement diminishes as $A_- \rightarrow A_+$. If we plot the maximum value of ψ as a function of A_- (figure 4) we see that the curve is roughly linear for much of the interval. There is an almost linear relationship between the amplitude and the sum of the tails for positive A_- . The relationship between the vortex amplitudes and the tails will be examined in more detail in section 5.

4.3. Vorticity tails with equal magnitudes and arbitrary phase

The last class of solutions that we will examine here are those with tails of the same magnitude but with no restriction on their alignment. Thus the possible extremes are again when the tails are aligned and of opposite sign, and when they are aligned and of the same sign. A sequence showing the transition between these extremes is shown in figure 5 for $\lambda = 6$ and a tail strength of $A_+ = A_- = 10$. This sequence shows a monotonically increasing amplitude for the vortices, but the phase difference is not monotonic. It decreases from the initial value $\Phi = \pi$, through 0 to a small negative number, $\Phi = -0.081\pi$. The phase difference then increases again, passing through 0 to $\Phi = 0.595\pi$ before decreasing again to 0 where the sequence ends with the same solution as found before. The curves of the maximum and minimum values of ψ are shown in figure 6 along with the corresponding curves for Φ ranging from $-\pi$ to 0. These curves consist of three sets of branches of solutions: the lower branches connected to the solutions which exist when $\Phi = \pm\pi$, the upper branch connected to the KD solution for $\Phi = 0$ and the middle branches that connect the ends of these two branches. We see that for some values of Φ multiple solutions are possible. For example, for $\Phi = 0$ there are 5 possible flows: the symmetric KD solution found previously on the upper branch, and a pair of solutions on each of the two other sets of branches of solutions. In each of these latter pairs the solutions are mirror images of each other. The width of the upper branch increases with increasing λ . The upper branch for $\lambda = 8$ and tail magnitude of 10 is also included in figure 6. This branch of solutions exists for almost the entire range of values of Φ .

The large amplitude of the upper branch is not strongly affected by the phase difference between the tails. The incoming vorticity is still swept into the vortices, but will take a longer or shorter route depending on the sense of rotation of the vortices and the phase difference. The vortices where this route is shorter tend to be relatively strong, while the counter rotating vortices with the longer path are relatively weak.

It may be anticipated that the upper and lower branches of solutions are stable and

the middle branch is unstable. However, no stability analysis of these solutions has yet been performed.

5. Link between tail and vortex amplitudes

One of the features that we can investigate is the maximum intensity of the vortices compared to the magnitude of the algebraic vorticity tails. This is illustrated in figure 7 for the solutions with both odd and even fundamental modes with $\lambda = 6$. There is a small degree of hysteresis in the odd case, but not in the even one. However there is a significant jump in the rate of increase in amplitude with tail strength when A_+ is around 2. Also shown in this figure is the corresponding curve for the even mode with $\lambda = 8$. Here there is clear hysteresis for the even mode. The details of the causes of this jump differ between the odd and even cases.

In the case of the solutions with the even fundamental mode (the KD solutions) the cause of the jump is that as the amplitude of the instabilities increases then the distribution of the vorticity changes. Instead of being confined to a region of thickness $\lambda^{-1/2}$ as shown by the linear large- λ asymptotics of KD, a region more extensive in the x -direction than the z -direction, the vorticity takes a more elliptical form with its major axis parallel to the z -axis. This results in the typical length scale for variations in the vorticity in the z -direction increasing, reducing the dissipation. This transition is shown by the vorticity distributions displayed in figure 8. These correspond to the flows shown in figures 5 and 6 of KD.

When the tails of vorticity are of the same magnitude but of opposite signs, as in section 4.2, the argument is slightly different. Again the initial configuration of vorticity conforms to that of the large λ asymptotics, but the rearrangement of vorticity has much to do with the vortex interactions discussed in section 4.2. These interactions move the vortices away from each other and thus significantly reduce the dissipation. In the KD case the vortices are unable to move away from each other. This extra mechanism allows for a more effective reduction in dissipation, thus the hysteresis is observed for lower values of λ .

The lower end of all the curves in figure 7 have slope 1. In this region the solutions are essentially linear and so this is the behaviour one would expect. However, the slope on the upper part of the curve for the solutions with the even fundamental mode (the solutions of KD) is less than 1, thus a doubling of the amplitude of the tail produces a smaller increase in the maximum of the stream function. Along this branch of solutions the distribution of the vorticity near the core of each vortex is well described by the large amplitude asymptotics of KD. However the asymptotic analysis presented there did not take into account any linkage between the cores of the vortices and the algebraically decaying vorticity tails. This linkage is a complex one. In figure 9 is shown the vorticity distribution for a KD vortex with $\lambda = 6$ and amplitude 5000. It shows how the tail of vorticity behaves as it approaches the large vortex core. There are three important regions. In addition to the vortex core, there is the region of algebraic decay for larger values of z . This extends almost all the way down to the the stagnation point in the flow above the region between the left pair of vortices. The vorticity then enters into a transition region where it is swept towards the edge of the vortex core. In the process it is squeezed into a narrow region which leads to enhanced lateral dissipation, leading to a reduction in the magnitude of the vorticity as it is swept towards the vortex. This vorticity then merges with the vortex core.

As the amplitude of the vortices grows, the position of the stagnation point moves further away. Thus for a given amplitude of tail the magnitude of the vorticity as it

enters the transition region will be lower. In addition the distance from this stagnation point to the vortex will be higher, giving more opportunity for viscous dissipation. These effects will lead to the ratio of the vorticity arriving in the core to the amplitude of the tail decreasing as the amplitude of the vortices increases.

One further feature of the distribution of the vorticity in figure 9 should be emphasised, and that is the large difference between the amplitude of the vorticity in the vortex cores and the vorticity being swept in from the tails. The magnitude of the vorticity in the core of this example exceeds 12000, while the local maximum in the incoming vorticity is just over 30. This weak feed of vorticity is required to maintain the steady vortices. If this supply was cut off the effect would be that the magnitude of the vortex would decay, but it may be anticipated that the rate of decay would be quite small.

The details of how all these regions link up is not clear. For larger values of λ the structure of the vortex cores is similar to those found by Moffatt, Kida & Ohkitani (1993) in the investigation of single vortices in a more general range of stagnation point flows. This similarity is especially strong for larger values of λ . One example of this similarity is shown in figure 10. The dissipation rate in the vortex cores displays the same structures that they found with their asymptotic analysis, and which have been observed elsewhere (for example, Kida & Ohkitani, 1992). In their analysis they are unable as yet to determine the structure of the decaying vorticity far from the vortex core. Their problem does not have the added complication of incoming vorticity that is present here.

6. Discussions

The understanding of how the steady-state periodic vortices in a stagnation point flow of Kerr & Dold (1994) are essentially driven by the inflow of vorticity from the far field has led to the discovery of further steady-state periodic vortex solutions. These do not have the original assumed symmetry of KD. We have only presented three new families of solutions here, and concentrated on one choice of λ . It is clear that there is a vast range of further solutions, many of which have not been investigated. However, the ones presented display many of the important features that would be observed in these other solutions.

In all these examples the vorticity is not confined to a finite region around the core of the vortices as in the case of the Burgers vortex (Burgers, 1948). For steady periodic vortices to exist there is a requirement for a supply of upstream vorticity. The need for this upstream supply of vorticity for steady vortices is not necessarily an onerous condition. The ratio of the magnitude of the vorticity at the vortex cores to that at even a moderate distance away from the plane $z = 0$ can be very large. Thus a seemingly weak level of disturbance in the upstream conditions in a typical experiment may result in the generation of large amplitude vortices.

One major area that has not yet been addressed is how these vortices would come into being. The temporal evolution of fully nonlinear vortices is beyond the scope of this paper. However the growth of linear instabilities is a simple extension of the current work. If one allowed for exponentially growing solutions with a nondimensional growth rate σ , then the equations for each mode become

$$a_n'' + \lambda z a_n' + (\lambda - \sigma - n^2)a_n = 0. \quad (6.1)$$

The analysis of this equation follows that of section 2, and all conclusions reached there will carry through for solutions with σ positive with minor changes. Thus exponentially growing solutions to the linear equations can only exist if there is an appropriate supply

of vorticity from afar. From this we can see that growing solutions will be a response to an increasing level of vorticity being supplied from some upstream source. If the far-field evolved in a way that resulted in the supply of vorticity increasing in some other way then the variables will not be separable and the appropriate partial differential equations would have to be solved.

The need for algebraic tails to the vorticity raises potential problems in situations where vortices are observed to grow in what are essentially stagnation point flows. One such case is the growth of secondary instabilities to Kelvin-Helmholtz rolls in a shear layer as discussed in KD. These secondary instabilities bear a close resemblance to the vortices discussed here and in KD. This leads one to expect that these instabilities require an increasing supply of vorticity from upstream. An investigation of this region for exponentially growing instabilities that has strictly localised vorticity is doomed to failure. This need for an upstream supply of vorticity may be satisfied by vorticity being supplied by the vortices in adjacent regions of stagnation point flow in the series of Kelvin-Helmholtz rolls. This possibility is investigated in Kerr (1997).

If one considers the kinetic energy of these disturbances a distinct difference is seen between these perturbations and those of Craik & Criminale (1986) or the fundamental modes of Lagnado, Phan-Thien & Leal (1984). If an energy per period per unit length in the y -direction of the perturbations is defined

$$E = \frac{1}{2} \int_{-\infty}^{\infty} \int_{-\pi}^{\pi} |\mathbf{u}|^2 dx dz, \quad (6.2)$$

then, with appropriate rescalings, the energy of the disturbances in the other works is infinite. In the examples here and in KD the velocities decay as $|z|^{-1+1/\lambda}$. Thus the integral of the energy will converge provided $\lambda > 2$. This is only slightly more restrictive than the condition for decaying solutions to exist, $\lambda > 1$. When $\lambda > 2$ this clearly indicates that the disturbances are extracting energy from the stagnation point flow, and are not just redistributing an infinite supply of energy.

The understanding of the periodic vortices in a stagnation point flow presented here and in Kerr & Dold (1994) has benefited from the appreciation of the requirement for algebraic tails to the vorticity in the upstream direction. This may seem to be a restriction in their applicability to real flows, however it could be considered to be a guide to where one should look for instability mechanisms. If these vortices are considered to be the signature of an upstream supply of vorticity then that is where one should look.

REFERENCES

- ARYSHEV, YU.A., GOLOVIN, V.A. & ERSIN, SH.A. 1981 Stability of colliding flows. *Fluid Dyn.* **16**, 755–759.
- BURGERS, J.M. 1948 A mathematical model illustrating the theory of turbulence. *Adv. Appl. Mech.* **1**, 171–199.
- CRAIK, A.D.D. & CRIMINALE, W.O. 1986 Evolution of wavelike disturbances in shear flows: a class of exact solutions of the Navier-Stokes equations. *Proc. R. Soc. Lond. A* **406**, 13–26.
- KERR, O.S. 1999 Streamwise vortex instabilities of Kelvin-Helmholtz rolls. In preparation.
- KERR, O.S. & DOLD, J.W. 1994 Periodic steady vortices in a stagnation point flow. *J. Fluid Mech.* **276**, 302–325. (herin referred to as KD)
- KIDA, S. & OHKITANI, K. 1992 Spatio-temporal intermittency and instability of a forced turbulence. *Phys. Fluids A* **4**, 1018–1027.
- LAGNADO, R.R., PHAN-THIEN, N. & LEAL, L.G. 1984 The stability of two-dimensional linear flows. *Phys. Fluids* **27**, 1094–1101.
- LIN, S.J. & G.M. CORCOS 1984 The mixing layer: deterministic models of a turbulent flow.

Part 3. The effect of plane strain on the dynamics of streamwise vortices. *J. Fluid Mech.* **141**, 139–178.

MOFFATT, H.K., KIDA, S. & OHKITANI, K. 1993 Stretched vortices — the sinews of turbulence; large-Reynolds-number asymptotics. *J. Fluid Mech.* **259**, 241–264.

Figure Captions

FIGURE 1. Sequence of flows with $A_+ = -A_-$ and $\Phi = 0$. The top row shows stream lines in the x - z plane for the full flow, the second row ω and the last ψ . In the last two rows the contour spacing is a sixth on the maximum modulus of ψ and ω respectively. The values of A_+ and the corresponding maxima of ψ and ω are (a) 2, 1.17, 3.11, (b) 20, 13.04, 37.30, (c) 30, 27.39, 73.93, (d) 35.6, 62.60, 161.3, (e) 35.6, 94.07, 238.4, (f) 34.6, 164.4, 408.9, (g) 40, 568.7, 1389.

FIGURE 2. Schematic diagram showing the effect of vortex interactions. (a) Initially vertical pairs of counter-rotating vortices interact to move sideways. (b) Horizontal rows no longer evenly spaced with the influence of nearest neighbours tending to make vortices move away from $z = 0$. (c) Pairs of vortices come to rest in region where the inward flow is sufficiently strong.

FIGURE 3. Sequence of flows with $A_+ = 10$ and A_- ranging from -10 to $+10$, with $\Phi = 0$. The top row shows stream lines in the x - z plane for the full flow, the second row ω and the last ψ . In the last two rows the contour spacing is a sixth on the maximum modulus of ψ and ω respectively. The values of A_- and the corresponding maxima of ψ and ω are (a) -10 , 5.90, 16.49, (b) -9 , 7.28, 19.53, (c) -7 , 12.14, 30.22, (d) -5 , 36.33, 89.08, (e) 0, 244.3, 594.3, (f) 5, 411.9, 1001, (g) 10, 562.6, 1368.

FIGURE 4. Graph of the maximum value of ψ of the vortices as a function of A_- , with $A_+ = 10$ and $\lambda = 6$.

FIGURE 5. Sequence of flows with $A_+ = A_-$ for a range of Φ . The top row shows stream lines in the x - z plane for the full flow, the second row ω and the last ψ . In the last two rows the contour spacing is a sixth on the maximum modulus of ψ and ω respectively. The values of Φ and the corresponding maxima are (a) π -10 , 5.90, 16.49, (b) 0.9π , 6.16, 17.21, (c) 0.6π , 21.30, 48.69, (d) -0.075π , 66.84, 152.0, (e) 0.25π , 113.6, 251.9, (f) 0.595π , 175.8, 403.5, (g) 0, 562.6, 1368.

FIGURE 6. Graph of the sizes of the maxima (solid line) and minima (dashed line) of ψ for $\lambda = 6$, $A_+ = A_- = 10$ and Φ ranging between $-\pi$ and π . Superimposed on each is the upper part of the corresponding curves for $\lambda = 8$ (dotted line).

FIGURE 7. Graphs of the maximum values of ψ for vortices as a function of the tail strength A_+ . The solid and dotted curves are for KD vortices ($A_+ = A_-$, $\Phi = 0$) with $\lambda = 6$ and $\lambda = 8$ respectively, while the dashed curve is for the vortices described in section 4.1 ($A_+ = -A_-$, $\Phi = 0$) with $\lambda = 6$.

FIGURE 8. Vorticity plots for the vortices corresponding to figures 5 and 6 of KD. These vortices have amplitudes (a) 2.5, (b) 10, (c) 40 and (d) 160. The contour spacing is a tenth of the maximum value of ω . In each case this maximum is (a) 5.696, (b) 23.16, (c) 75.13, and (d) 388.8.

FIGURE 9. Plots of the (a) streamlines and (b) vorticity of the upper half of vortices with $\lambda = 6$ and amplitude 5000. The contour intervals in (b) are 1216 near the vortex cores, and 10 elsewhere.

FIGURE 10. Dissipation for KD vortex with $\lambda = 50$ and amplitude 80.

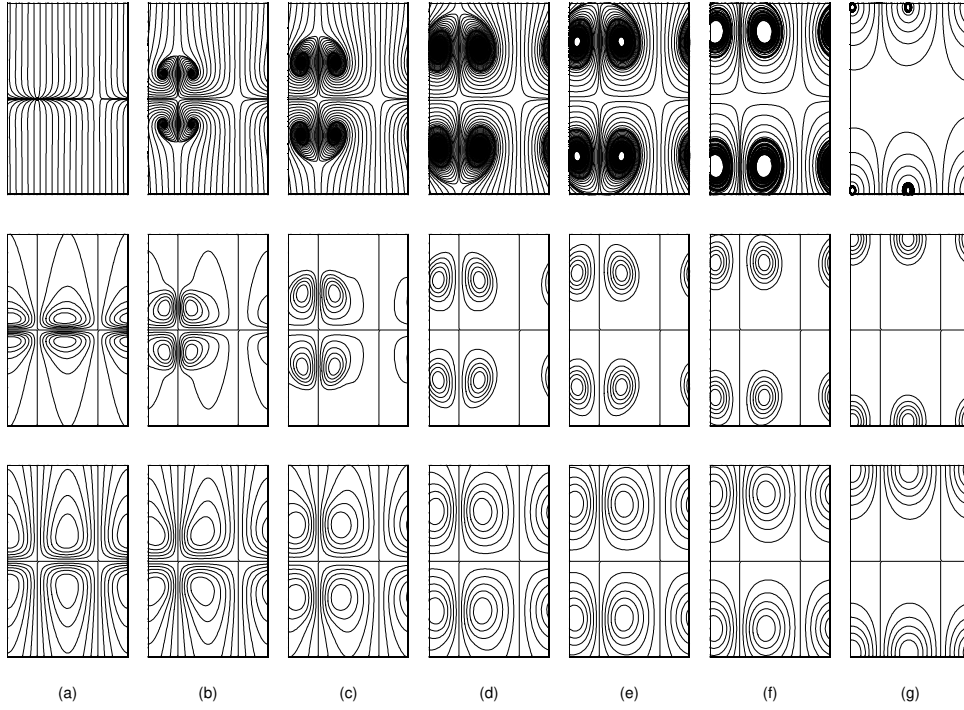


FIGURE 1. Sequence of flows with $A_+ = -A_-$ and $\Phi = 0$. The top row shows streamlines in the x - z plane for the full flow, the second row ω and the last ψ . In the last two rows the contour spacing is a sixth of the maximum modulus of ψ and ω respectively. The values of A_+ and the corresponding maxima of ψ and ω are (a) 2, 1.17, 3.11, (b) 20, 13.04, 37.30, (c) 30, 27.39, 73.93, (d) 35.6, 62.60, 161.3, (e) 35.6, 94.07, 238.4, (f) 34.6, 164.4, 408.9, (g) 40, 568.7, 1389.

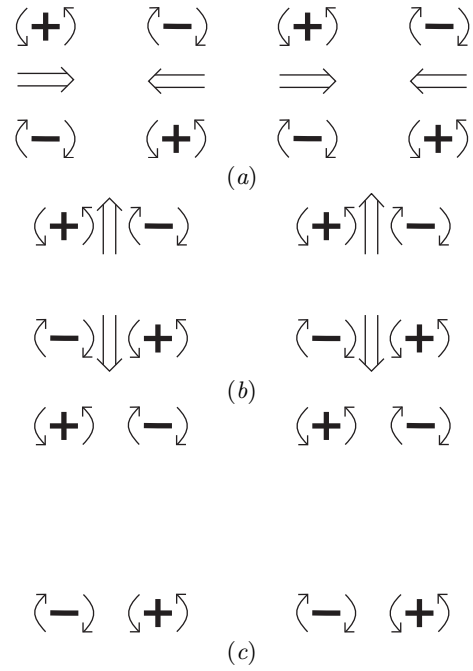


FIGURE 2. Schematic diagram showing the effect of vortex interactions. (a) Initially vertical pairs of counter-rotating vortices interact to move sideways. (b) Horizontal rows no longer evenly spaced with the influence of nearest neighbours tending to make vortices move away from $z = 0$. (c) Pairs of vortices come to rest in region where the inward flow is sufficiently strong.

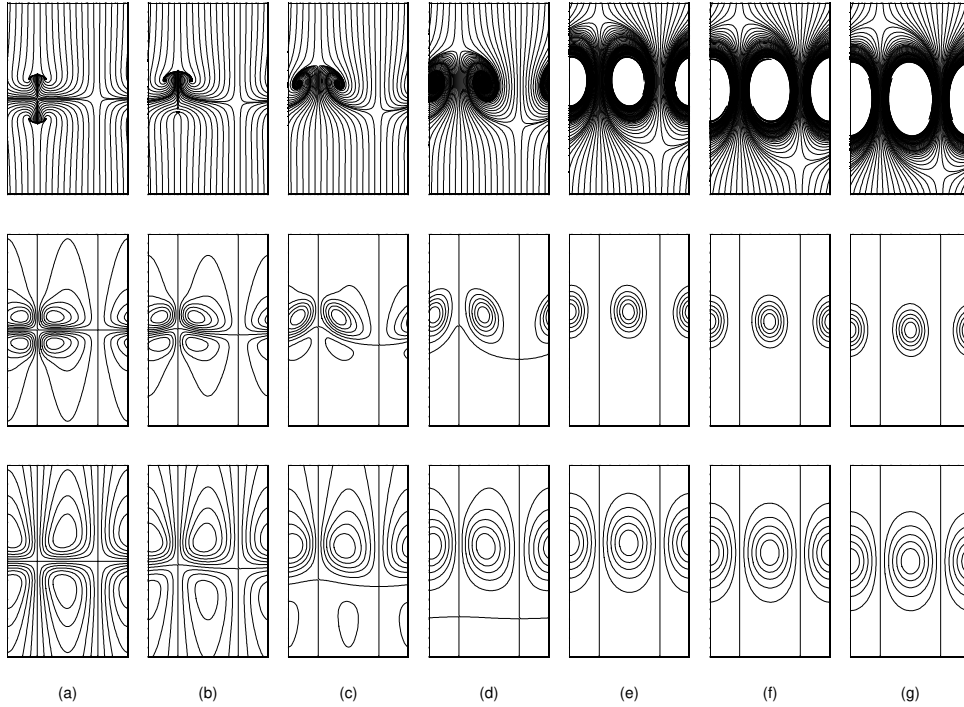


FIGURE 3. Sequence of flows with $A_+ = 10$ and A_- between -10 and $+10$, with $\Phi = 0$. The top row shows streamlines in the x - z plane for the full flow, the second row ω and the last ψ . In the last two rows the contour spacing is a sixth of the maximum modulus of ψ and ω respectively. The values of A_- and the corresponding maxima of ψ and ω are (a) -10 , 5.90 , 16.49 , (b) -9 , 7.28 , 19.53 , (c) -7 , 12.14 , 30.22 , (d) -5 , 36.33 , 89.08 , (e) 0 , 244.3 , 594.3 , (f) 5 , 411.9 , 1001 , (g) 10 , 562.6 , 1368 .

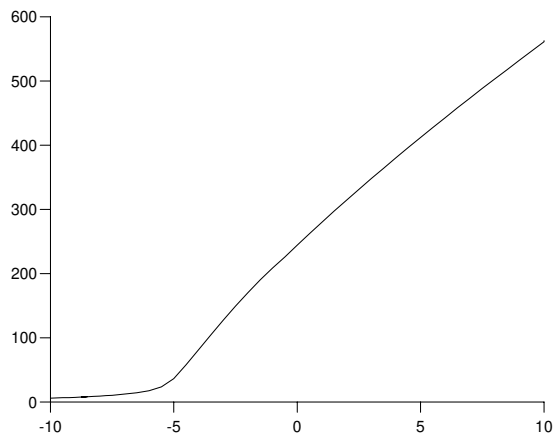


FIGURE 4. Graph of the maximum value of ψ of the vortices as a function of A_- , with $A_+ = 10$ and $\lambda = 6$.

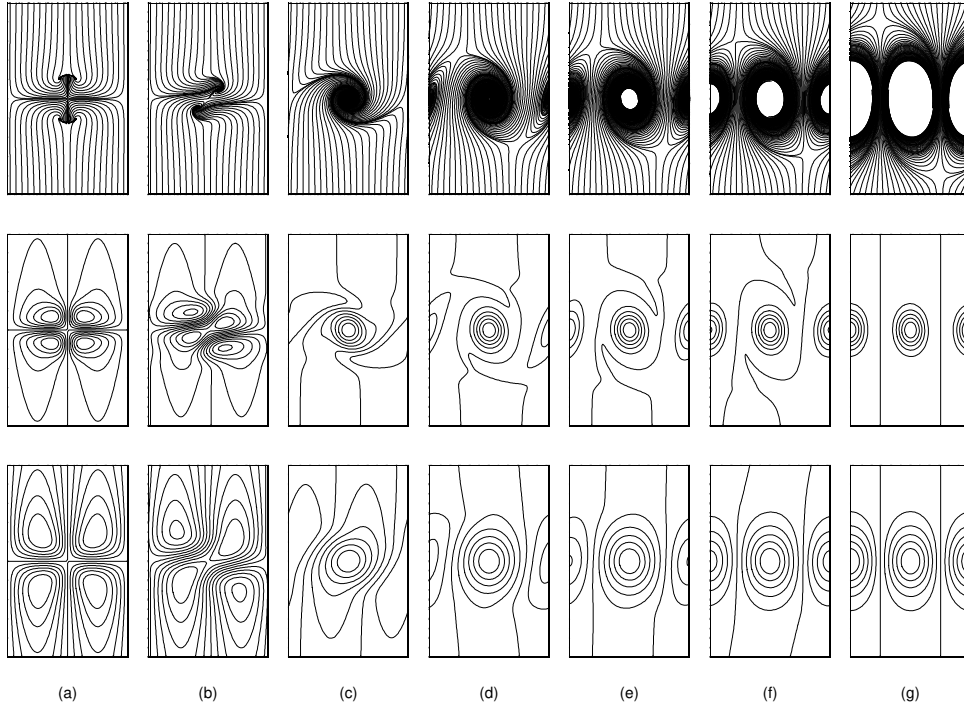


FIGURE 5. Sequence of flows with $A_+ = A_- = 10$ for a range of Φ . The top row shows streamlines in the $x-z$ plane for the full flow, the second row ω and the last ψ . In the last two rows the contour spacing is a sixth on the maximum modulus of ψ and ω respectively. The values of Φ and the corresponding maxima are (a) π , 5.90, 16.49, (b) 0.9π , 6.16, 17.21, (c) 0.6π , 21.30, 48.69, (d) -0.075π , 66.84, 152.0, (e) 0.25π , 113.6, 251.9, (f) 0.595π , 175.8, 403.5, (g) 0, 562.6, 1368.

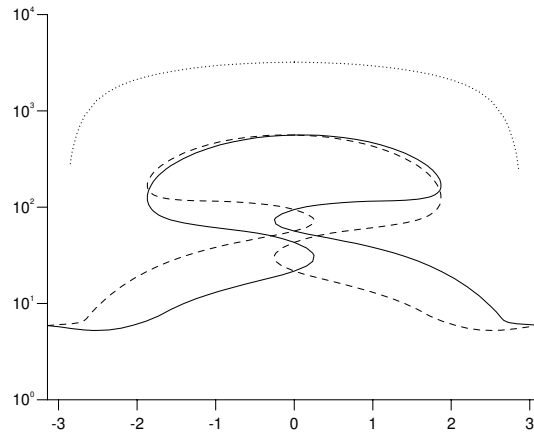


FIGURE 6. Graph of the sizes of magnitudes of the maxima (solid line) and minima (dashed line) of ψ for $\lambda = 6$, $A_+ = A_- = 10$ and Φ ranging between $-\pi$ and π . The dotted line shows the uppermost part of the corresponding curves for $\lambda = 8$.

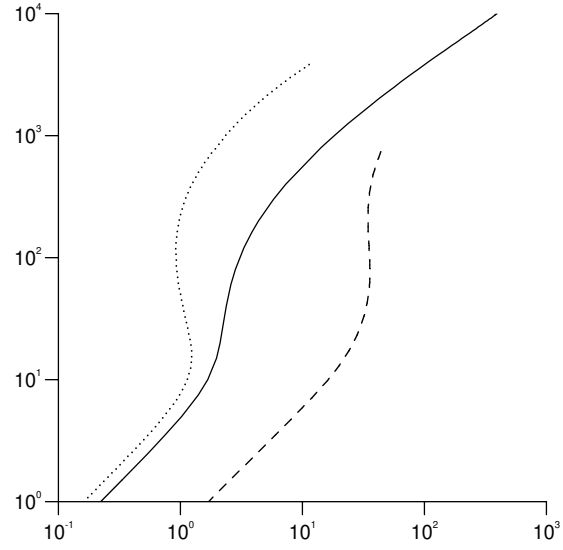


FIGURE 7. Graphs of the maximum values of ψ for vortices as a function of the tail amplitude A_+ . The solid and dotted curves are for KD vortices ($A_+ = A_-$, $\Phi = 0$) with $\lambda = 6$ and $\lambda = 8$ respectively, while the dashed curve is for the vortices described in section 4.1 ($A_+ = -A_-$, $\Phi = 0$) with $\lambda = 6$.

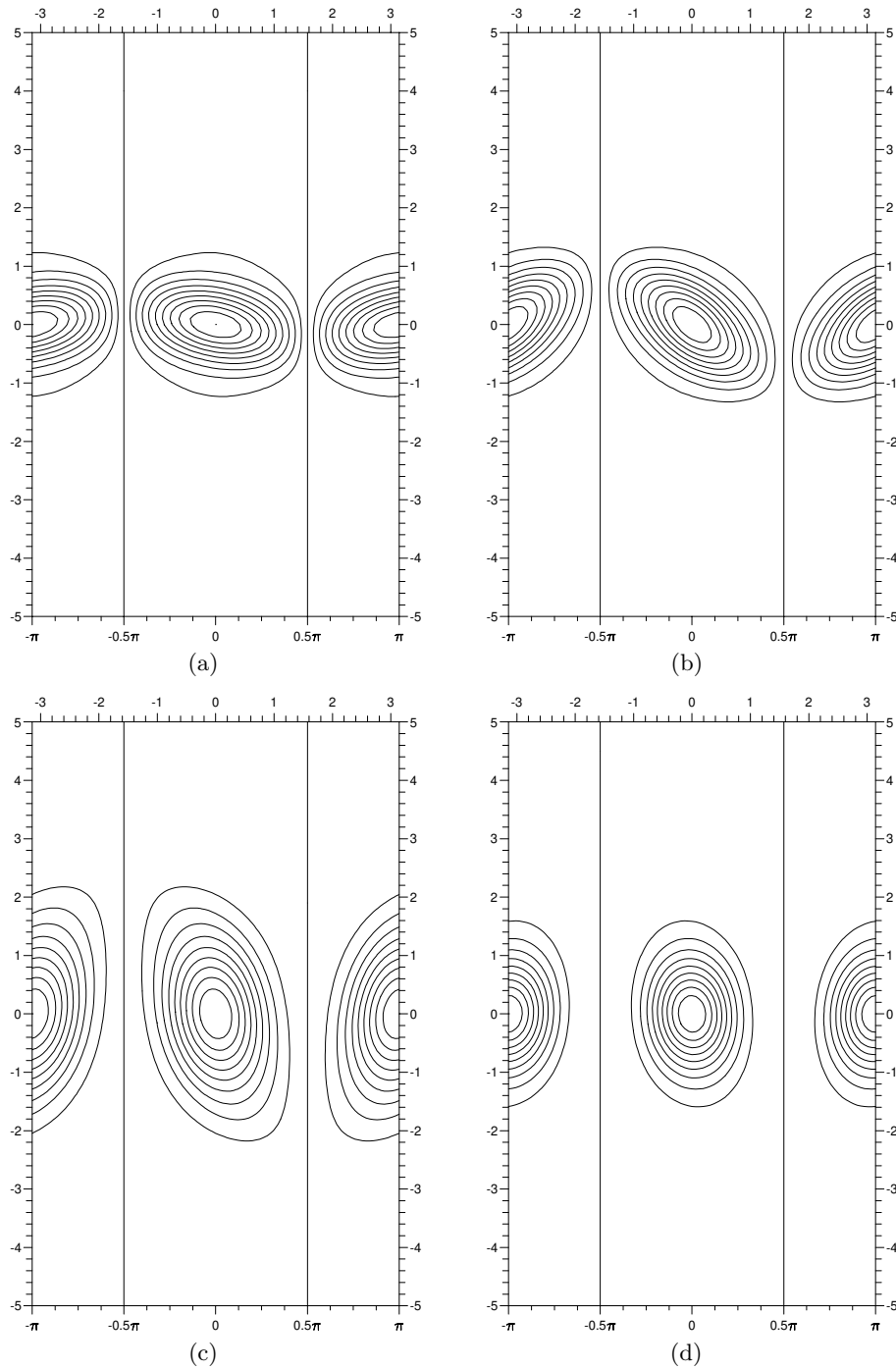


FIGURE 8. Vorticity plots for the vortices corresponding to figures 5 and 6 of KD. These vortices have amplitudes (a) 2.5, (b) 10, (c) 40 and (d) 160. The contour spacing is a tenth of the maximum value of ω . In each case this maximum is (a) 5.696, (b) 23.16, (c) 75.13, and (d) 388.8.

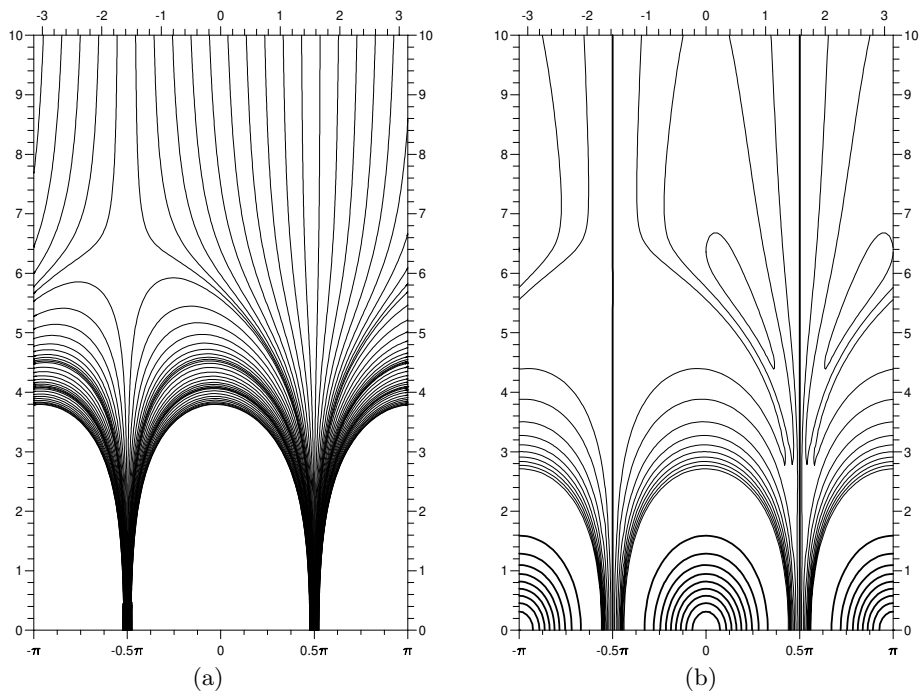


FIGURE 9. Plots of the (a) streamlines and (b) vorticity of the upper half of vortices with $\lambda = 6$ and amplitude 5000. The contour intervals in (b) are 1216 near the vortex cores, and 10 elsewhere.

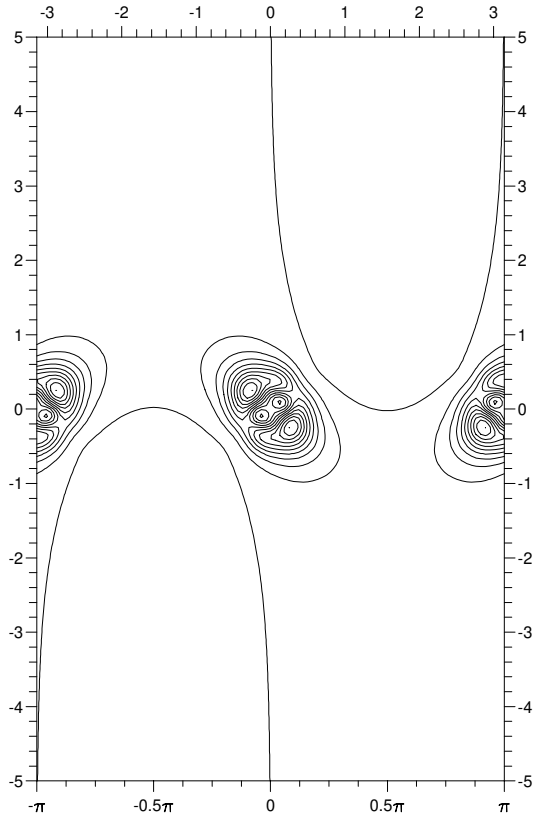


FIGURE 10. Dissipation for KD vortex with $\lambda = 50$ and amplitude 80.